STRUCTURAL CONTROL AND HEALTH MONITORING
Struct. Control Health Monit. 2009; **16**:549–563
Published online 26 February 2009 in Wiley InterScience (www.interscience.wiley.com). DOI: 10.1002/stc.293

Benchmark structural control problem for a seismically excited highway bridge—Part III: Phase II Sample controller for the fully base-isolated case

Satish Nagarajaiah[1,*,†,‡], Sriram Narasimhan[2,§], Anil Agrawal[3,‡] and Ping Tan[4,‡]

[1]*Deptartment of Civil and Environmental Engineering and Mechanical Engineering and Material Science, Rice University, Houston, TX 77005, U.S.A.*
[2]*Deptartment of Civil and Environmental Engineering, University of Waterloo, Waterloo, Ont., Canada*
[3]*The City College of the City University of New York, New York, NY 10031, U.S.A.*
[4]*Guangzhou University, China*

SUMMARY

This paper presents the fully base-isolated highway bridge benchmark problem. The highway bridge benchmark problem consists of two phases: (1) Phase I—the bridge deck being base isolated only at the abutments and the center bent being integral with the pier (without isolation), and (2) Phase II—the bridge deck being fully base isolated at both the bent/pier and abutment locations. In both phases of the highway bridge benchmark, the objective is to augment the performance of the isolation system using supplemental control strategies. The problem definition (Part I) as well as a sample controller (Part II) for Phase I of the study has been presented in the companion papers. The focus of this paper is to present the fully base-isolated highway bridge and sample Lyapunov semiactive controller (Part III). As-built structural designs of the 91/5 overcrossing in Orange county in Southern California are used to develop the finite-element model for this benchmark based on Phase I. The nonlinear analysis tool and the controller interface have been developed in MATLAB. The bridge is isolated using nonlinear elastomeric bearings with a lead core. Magneto-rheological (MR) dampers are used to control the seismic response of the bridge. The MR dampers are installed at the isolation level at 10 locations over the abutments and bent/pier locations, each location consisting of an orthogonal pair of dampers to control the responses in both directions. The outputs allowed in the benchmark problem definition are used to design the controller and the velocity and displacement measurements if required are obtained by integrating accelerations using a filter, which simulates integration. Detailed comparisons of benchmark performance indices for the fully base-isolated bridge with sample semiactive controllers and passive strategies are performed in comparison with the uncontrolled case, for a set of strong near-field earthquakes. The sample Lyapunov semiactive controller is shown to reduce the isolator and mid-span displacements. The modeling and sample control designs demonstrated in this paper can be used to form the basis for studying a wider variety of active and

*Correspondence to: S. Nagarajaiah, Department of Civil and Environmental Engineering and Mechanical Engineering Material Science, Rice University, Houston, TX 77005, U.S.A.
†E–mail: nagaraja@rice.edu
‡Professor.
§Assistant Professor.

Received 2 April 2008
Revised 10 September 2008
Accepted 16 September 2008

semiactive control strategies—to be developed by the participants in the benchmark study—for fully base-isolated highway bridges. Copyright © 2009 John Wiley & Sons, Ltd.

KEY WORDS: benchmark problem; fully base-isolated highway bridge; lead-rubber bearings; MR dampers; Lyapunov sample controller

INTRODUCTION

Recent earthquake activities worldwide and the resulting damage have reinforced the need and urgency to protect civil infrastructure and its occupants against severe earthquakes. In order to reduce the vulnerability of building and bridge structures to severe earthquakes, 'smart' base-isolated structures, where the performance of the base isolation system is improved by adding semiactive variable stiffness and damping devices, have been proposed and studied by various researchers [1–20]. Over the last decade, the ASCE Structural Control and Monitoring Committee and Task Group on Benchmark Problems, the U.S. Panel on structural control and IASCM (International Association for Structural Control and Monitoring) have developed a series of benchmark problems in structural control. The benchmark studies have addressed the problem of control on a variety of structure and loading types such as seismic and wind-excited buildings and seismically excited long-span cable-stayed bridges [21–26]. Recently concluded nonlinear base-isolated building benchmark studies [7,12,27–30], in which more than two dozen researchers presented their findings, also focused on smart base-isolated structures, more specifically on buildings. A key conclusion from this study was the need of further research into effectively controlling the response of nonlinear base-isolated structures. Specifically, it was found that although a majority of passive, semiactive and active controllers are effective in reducing the isolation level displacements, the superstructure accelerations and drifts still posed challenges for nonlinear isolation systems.

Highway crossings are critical infrastructure as they serve as major access and evacuation routes during and after catastrophic events. It is extremely critical that these bridges remain operational following severe earthquakes. In order to facilitate comparisons between various control strategies for base-isolated highway bridges, a new benchmark problem has been developed [31] by the U.S. Panel and ASCE structural control and monitoring committees. The highway bridge benchmark provides a valuable test-bed to further improve the controller designs and address the challenges of reducing the response of highway bridges with nonlinear isolation systems. The highway benchmark study has been designed to include passive, semiactive and active control strategies. Sample active, semiactive and passive controllers have been provided for the Phase I study for the partially isolated case [31,32]. Passive and semiactive sample control strategies are presented in this Phase II study for the fully isolated case.

As mentioned earlier the base isolation system is studied in two phases in this benchmark study. In Phase I base isolation is at the abutments only, with four nonlinear lead-rubber bearings (LRB) utilized to isolate the deck at each abutment. In Phase I, the center bent and pier connections are not isolated and are expected to exhibit inelastic behavior under severe ground motions [31]. In Phase II, the bridge deck is isolated at the abutments and the center bent/piers as well as shown in Figure 1. In Phase II, which is presented in this paper, a total of 20 control devices (10 in each direction) are placed at the isolator locations as shown in Figure 2. The

DOI: 10.1002/stc

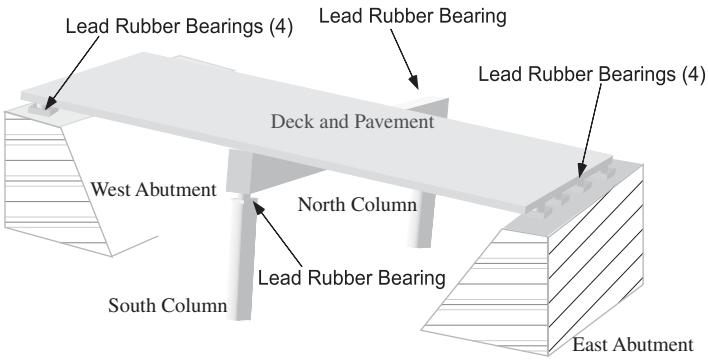

Figure 1. Schematic of the highway bridge benchmark (skew not shown).

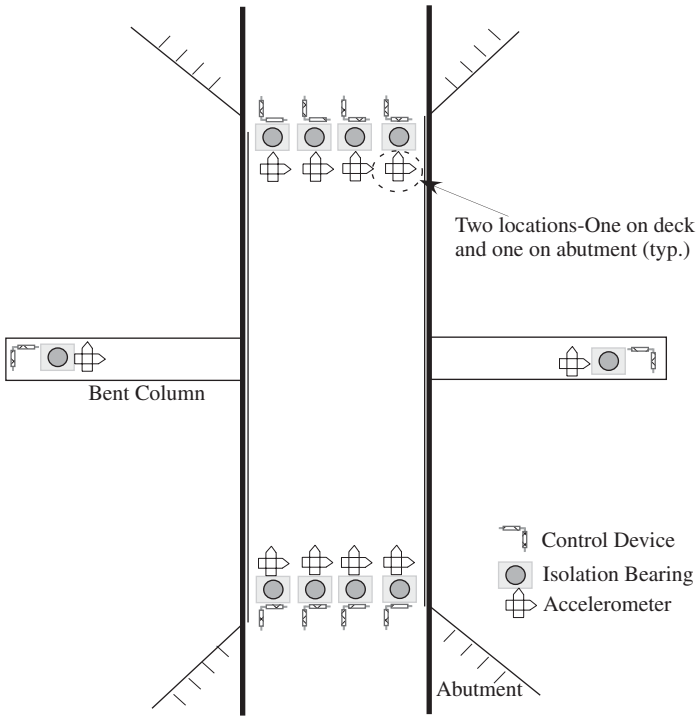

Figure 2. Locations of control devices and sensors on the bridge (skew not shown).

control devices are expected to augment the performance of the isolation system by providing additional control action and energy dissipation.

The highway bridge benchmark model is based on the newly constructed 91/5 highway bridge in southern California [5]. It is a continuous two-span, cast-in-place prestressed concrete box-girder bridge. The Whittier–Ellsinore fault is 11.6 km (7.2 miles) to the northeast, and the Newport–Inglewood fault zone is 20 km (12.5 miles) to the southwest of the bridge. The bridge has two spans, each of 58.5 m (192 ft) long spanning a four-lane highway and has two abutments

DOI: 10.1002/stc

skewed at 33°. The width of the deck along east span is 12.95 m (42.5 ft) and it is 15 m (49.2 ft) along west direction. The cross section of the deck consists of three cells. The deck is supported by a 31.4 m (103 ft) long and 6.9 m (22.5 ft) high prestressed outrigger, which rests on two pile groups, each consisting of 49 driven concrete friction piles. The columns are approximately 6.9 m (22.5 ft) high. Additional details of the bridge are presented in the definition paper [5,31] and a schematic is given in Figure 1. For full details of the bridge the reader is referred to the companion paper [31].

A sample semiactive Lyapunov controller using magneto-rheological (MR) dampers [33] is presented for the Phase II benchmark. MR dampers have been studied extensively in the literature for the control of both linear and nonlinear structures [33,34]. The basic idea of using MR dampers is to effectively switch the level of nonlinear damping in response to earthquake excitations so that the resulting performance is better than an equivalent passive damper. In this study, a total of 20 MR dampers are installed in the isolation system locations, each location consisting of an orthogonal pair of MR dampers to control the responses in both directions as shown in Figure 2. The switching law for the dampers is developed using a Lyapunov formulation. The outputs allowed in the benchmark problem definition paper [31] are used to design the controller, and the velocity and displacement measurements if required are obtained by integrating accelerations using a filter, which simulates integration. Detailed comparisons of benchmark performance indices for the fully base-isolated bridge with sample semiactive controllers and passive controllers are performed in comparison with the uncontrolled case, for a set of strong near-field earthquakes. The sample Lyapunov semiactive controller is shown to reduce the isolator and mid-span displacements.

In this paper the structural model is presented first, followed by the Lyapunov controller formulation. The controller implementation and device descriptions are presented next, followed by numerical simulation results. Finally, key conclusions of this paper are presented. The modeling and sample control designs demonstrated in this paper can be used to form the basis for studying a wider variety of passive, semiactive and active control strategies—to be developed by the participants in the benchmark study—for fully base-isolated highway bridge problems. The controller developed herein is not intended to be competitive; it provides a set of programs and tools to aid participants to design competitive controllers for the Phase II highway-isolated bridge benchmark. However, it is anticipated that the participant would compare the results of their controllers with the results from the sample controller presented in this paper.

STRUCTURAL MODEL

A full three-dimensional finite-element model was developed in ABAQUS [35] in order to compute the structural properties of the system. Complete details of this model along with their dynamic properties are described in the definition paper [31]. In addition to a total of 108 nodes, 4 rigid links, 70 beam elements, 24 springs and 27 dashpots, 10 user-defined bearing elements are modeled. The deck structure elements are assumed to be linear and the element stiffness and mass matrices are derived from the finite-element model and assembled at the nodes using lumped mass and stiffness approximation. The nonlinear elements are added to the linear elastic deck elements and the augmented model is used for evaluating structural responses.

All element mass matrices and initial elastic element stiffness matrices obtained in ABAQUS are summed at nodal masses to assemble global stiffness and mass matrices within MATLAB

DOI: 10.1002/stc

environment, and then the nonlinear elements are modeled for generating the evaluation model. Each nodal mass of the deck and bent is assigned six dynamic degrees of freedom (DOF). The deck-ends and abutments, which are assumed to be infinitely rigid in plane, are modeled using three master DOF (two translational and one torsional DOF). The full nonlinear model of the bridge has 430 DOF. This model is used as the evaluation model of the bridge.

The equations of motion for the bridge is given by

$$\mathbf{M}\ddot{\mathbf{U}}(t) + \mathbf{C}\dot{\mathbf{U}}(t) + \mathbf{K}(t)\mathbf{U}(t) = -\mathbf{M}\eta\ddot{\mathbf{U}}_{\mathrm{g}}(t) + \mathbf{b}\mathbf{F}(t) \tag{1}$$

where $\mathbf{M}$ is the assembled mass matrix consisting of all the nodal masses, $\mathbf{C}$ is the assembled stiffness matrix and $\mathbf{K}(t)$ is the assembled stiffness matrix consisting of both the linear and nonlinear parts. The vector η contains the loadings for the ground acceleration, and the matrix $\mathbf{b}$ is the control force influence matrix. The vector $\mathbf{F}$ is the control force generated by the control devices. Equation (1) is solved using Newmark's method in an incremental form and the details are given in the definition paper [31].

The global damping matrix C can be expressed as a combination of the distributed 'inherent' damping in the structure and soil radiation damping. The inherent damping of the superstructure is assumed to be a function of the mass and initial elastic stiffness matrix of the superstructure. The Raleigh damping parameters are computed by assuming a 5% modal damping ratio in the first and second modes.

The nonlinear moment–curvature behavior of the two center columns is modeled by a bilinear hysteresis model. For simplification, the force–deformation relationships for axial, shear and torsional behavior are assumed to be linear and only two bending moment–curvature relationship is considered to be bilinear. The interaction between the axial load and bending moment during earthquake motions is not included. In addition, the nonlinear responses in both directions are considered to be uncoupled. This assumption is reasonable since the responses of columns are dominated by bending.

A concentrated plasticity model is implemented for modeling the material nonlinearity of the bent column. The plastic deformations over an element are assumed to be concentrated at the ends of the member. The moment–curvature relationship in both directions is idealized as bilinear and composed of two components: linear and elasto-plastic component. The elastic behavior remains unchanged, while the moments and shears of the elasto-plastic member are the combination of the end forces of the components according to the state of yield.

The bridge deck is isolated at the abutments and the center bent/piers as well as shown in Figures 1 and 2. A total of 10 LRB are used to isolate the bridge deck, placed at the locations shown in Figure 2. The four isolators between the deck and the abutment are located at the east and the west abutments. The isolators between the outrigger bent and the piers are placed on top of the south column and the north column, as shown in Figures 1 and 2.

The isolation system is modeled using a bilinear force–deformation relationship in both x and y directions as follows [31]:

$$\begin{aligned} F_x &= K_{px}U_x + (K_{ex} - K_{px})\bar{U}_x \\ F_y &= K_{py}U_y + (K_{ey} - K_{py})\bar{U}_y \end{aligned} \tag{2}$$

In Equation (2), F_x is the restoring force of the isolation bearings in the x direction, F_y is the restoring force of isolation bearings in the y direction, K_p is the post-yield stiffness of isolation

DOI: 10.1002/stc

bearings (x and y directions indicated by the corresponding subscripts), K_e is the pre-yield stiffness of isolation bearings and $\bar{U}$ is the yield displacement of bearings.

A total of 20 control devices (10 in each direction) are placed at the isolator locations as shown in Figure 2. These consist of four locations (two devices per location) between the deck and each abutment and two locations on the center columns (one on each side of the deck).

For the Phase I controller design, a linearized reduced-order model based on modal reduction techniques [32] is derived from the full-order evaluation model. The resulting reduced-order model is found to capture the dynamics of the full-order model accurately in the modes of interest. The control-oriented model is given as

$$\dot{\mathbf{x}}^r = \mathbf{A}_\mathrm{r}\mathbf{x}^r + \mathbf{B}_\mathrm{r}\mathbf{u} + \mathbf{E}_\mathrm{r}\ddot{\mathbf{u}}_\mathrm{g} \tag{3}$$

$$\mathbf{y}_z = \mathbf{C}_\mathrm{r}^z\mathbf{x}^r + \mathbf{D}_\mathrm{r}^z\mathbf{u} + \mathbf{F}_\mathrm{r}^z\ddot{\mathbf{u}}_\mathrm{g} \tag{4}$$

$$\mathbf{y}_m = \mathbf{C}_\mathrm{r}^m\mathbf{x}^r + \mathbf{D}_\mathrm{r}^m\mathbf{u} + \mathbf{F}_\mathrm{r}^m\ddot{\mathbf{u}}_\mathrm{g} + v \tag{5}$$

where the subscript r in Equations (3)–(5) refers to the reduced model. In the above equations, $\mathbf{x}$ refer to the states of the system, $\mathbf{A}$, $\mathbf{B}$ and $\mathbf{E}$ are the system state matrices and $\ddot{\mathbf{u}}_\mathrm{g}$ is the ground acceleration vector in two directions. The regulated output $\mathbf{y}_z$ and the measurement output $\mathbf{y}_m$ equations are given in Equations (4) and (5), respectively. Matrices $\mathbf{C}$, $\mathbf{D}$ and $\mathbf{F}$ are mapping matrices of appropriate dimensions and v denotes the measurement noise. The above reduced-order state-space form has been used to develop the active and sem-iactive controllers (H_2/LQG) formulation in Phase I. However, for Phase II of the study, the outputs are directly used to implement a controller as described next, and a reduced-order form is not necessary.

A total of six earthquake motions are used to excite the bridge in two directions. Two components, fault-normal and fault-parallel components, of the six earthquakes are used to excite the bridge in both directions. The earthquakes used in this study are North Palm Springs (1986), TCU084 component of Chi-Chi earthquake, Taiwan (1999), El Centro component of 1940 Imperial Valley earthquake, Rinaldi component of Northridge earthquake (1994), Bolu component of Duzce earthquake in Turkey and Nishi-Akashi component of Kobe (1995) earthquake. These earthquakes are chosen to represent a broad range of ground motion intensities (PGA ranges from $0.22g$ for El Centro to $0.82g$ for Turkey-Bolu), soil classes (A–D) and spectral content.

SEMIACTIVE LYAPUNOV CONTROL ALGORITHM

Base-isolated structures can be idealized as single DOF (SDOF) nonlinear oscillators. The Lyapunov semiactive control algorithm [14,28] utilized in the control of the highway bridge is developed based on energy principles for a general ground-excited spring-mass-dashpot system with time-varying damping. For a general SDOF system consisting of mass m, stiffness k and a time-varying damping $c(t)$, the equations of motion can be written in state space as follows:

$$\dot{\mathbf{X}} = \mathbf{A}\mathbf{X} - \mathbf{B}c(t)\dot{u}_\mathrm{r} + \mathbf{B}ku_\mathrm{g} \tag{6}$$

where

$$A = \begin{bmatrix} 0 & 1 \\ \dfrac{-k}{m} & 0 \end{bmatrix} \tag{7}$$

DOI: 10.1002/stc

$$\mathbf{B} = \begin{Bmatrix} 0 \\ \dfrac{1}{m} \end{Bmatrix} \tag{8}$$

$$\mathbf{X} = \begin{Bmatrix} u_a \\ \dot{u}_a \end{Bmatrix} \tag{9}$$

In the above equations, u_a and $\dot{u}_a$ denote the absolute displacement and absolute velocity, respectively, u_r is the relative displacement and u_g denotes the ground displacement. A positive-definite scalar Lyapunov function (V) is constructed using the states defined in Equation (6) as follows:

$$V = \tfrac{1}{2}\sigma^T(X)\sigma(X) \tag{10}$$

where

$$\sigma(\mathbf{X}) = \mathbf{P}^T X = [\sqrt{k} \quad \sqrt{m}] \begin{Bmatrix} u_a \\ \dot{u}_a \end{Bmatrix} \tag{11}$$

where $\mathbf{P}$ is a positive vector.

Hence, the Lyapunov function V can now be written as

$$V = \tfrac{1}{2}ku_a^2 + \sqrt{k}\sqrt{m}u_a\dot{u}_a + \tfrac{1}{2}m\dot{u}_a^2 \tag{12}$$

where the first term represents the total strain energy in the spring, the second term represents the dissipated energy and the third term represents the total kinetic energy.

The Lyapunov derivative can be written as

$$\dot{V} = \sigma(\mathbf{X})\mathbf{P}^T\mathbf{B}\dot{u}_r\left(-c(t) + \frac{1}{\dot{u}_r}(\sqrt{k}\sqrt{m}\dot{u}_a - ku_r)\right) \tag{13}$$

For $\dot{V}$ to be negative, the following condition should be satisfied:

$$c(t) = \begin{cases} c_2 \text{ or } c_{\max} & (\sqrt{k}u_a + \sqrt{m}\dot{u}_a)\dot{u}_r > 0 \\ c_1 \text{ or } c_{\min} & (\sqrt{k}u_a + \sqrt{m}\dot{u}_a)\dot{u}_r < 0 \end{cases} \tag{14}$$

Equation (14) can also be written as

$$c(t) = \begin{cases} c_2 \text{ or } c_{\max} & (\omega_n u_a + \dot{u}_a)\dot{u}_r > 0 \\ c_1 \text{ or } c_{\min} & (\omega_n u_a + \dot{u}_a)\dot{u}_r < 0 \end{cases} \tag{15}$$

where $\omega_n = \sqrt{k/m}$, $u_a(t)$ is the absolute displacement and $\dot{u}_r(t)$ is the relative velocity of the structure.

It is worth noting that since there are no restrictions on the magnitude of the elements of the vector $\mathbf{P}$ in Equation (11) (as long as they are positive real numbers), the algorithm is robust to uncertainties in the system parameters, namely k and m. For the ensuing simulations, the value of $\omega_n = 1.68$ rad/s corresponding to the post-yield period of the isolation system is used.

DOI: 10.1002/stc

CONTROLLER IMPLEMENTATION

Two types of control devices are implemented in Phase II of this study: passive nonlinear dampers and MR dampers. The control devices are placed between the abutments/piers and the deck at the 20 locations shown in Figures 1 and 2. For passive control implementation, the force generated in the device depends only on the displacement and/or velocity between the connection points of the damper. The passive nonlinear damper used in the study generates the control force according to the following relationship [32]:

$$f = c_\alpha |\dot{u}_r|^\alpha \mathrm{sgn}(\dot{u}_r) \tag{16}$$

where c_α is an experimentally determined damping coefficient and $\dot{u}_r$ is the velocity across the piston of the damper. α determines the nature of the nonlinearity of the damper and has a value between 0 and 1, where the extremes correspond to a friction and linear viscous damper, respectively. For this study, $\alpha = 0.6$ is used. To simulate the Lyapunov controller developed in the previous section, MR dampers are used at the device locations shown in Figure 2. The MR dampers are modeled using the Bouc–Wen hysteretic model as explained in the Phase I study of the highway benchmark [32,34,36]. The control force generated in the MR damper is given by

$$f = c_o \dot{u}_r + \alpha z \tag{17}$$

where c_o is a viscous damping coefficient and z is a dimensionless hysteretic variable calculated by solving the nonlinear differential equation [36]

$$\dot{z} = -\gamma |\dot{u}_r| z |z|^{n-1} - \beta \dot{u}_r |z|^n + A \dot{u}_r \tag{18}$$

where γ, n, β and A govern the nature of the hysteresis in the damper [34]. The magnitude of the control force in the MR damper is adjusted by varying the applied external voltage. This is represented mathematically by the voltage dependence of the damper parameters, c_0 and α. These functional relationships along with the values of these parameters have been presented in the Phase I study of the highway benchmark [32].

The control law in Equation (15) requires both absolute and relative velocity and displacement measurements at the device locations. In order to obtain these quantities, the absolute acceleration measurements at the device locations are integrated successively using a filter that simulates an integrator [7]. The overall implementation scheme is given in Figure 3 and the SIMULINK model that is distributed to the participants of this study is shown in Figure 4.

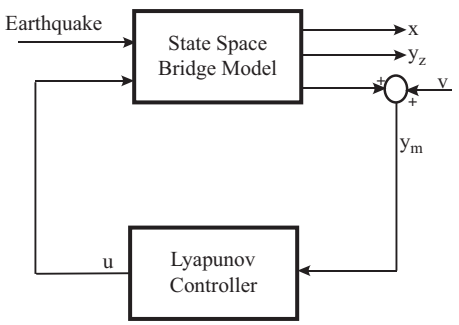

Figure 3. Overall numerical implementation.

DOI: 10.1002/stc

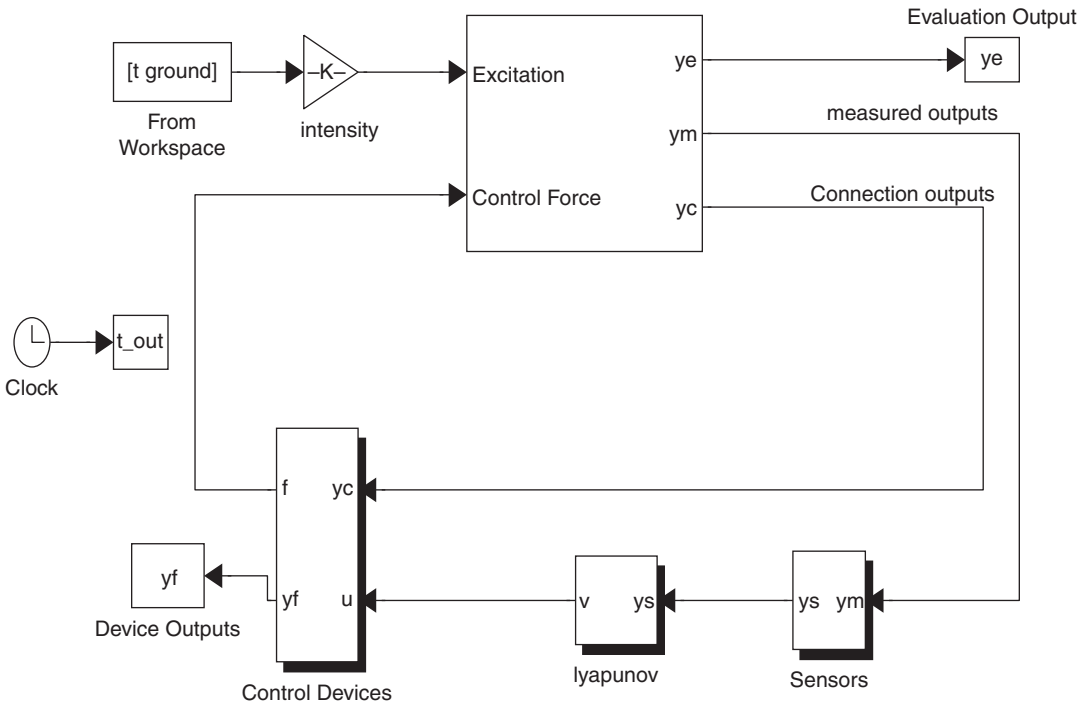

Figure 4. MATLAB/SIMULINK semiactive control model.

NUMERICAL SIMULATION STUDY

A set of 21 performance indices has been developed to assess the effectiveness of control schemes comprehensively [31]. These performance indices measure the impact of the control strategy in terms of various structural responses such as displacement, moment and accelerations at key locations in the structure. These performance indices are summarized in Table I and readers are referred to the definition paper [31] for more details.

Both the semiactive Lyapunov and passive control strategies are implemented for the Phase II benchmark structure. The highway bridge is modeled as a multi-degree of freedom system; however, the deck system is rigid in plane and the deck isolated with the LRB isolation system will essentially behave like an SDOF. Hence, the bridge deck is modeled using three master DOF (two translational and one torsional DOF).

MR dampers [33] are used as control devices at the locations shown in Figure 1. The parameters of the MR damper are described in the sample control design of the Phase I benchmark definition paper [32]. The results of the numerical study in terms of the performance indices and time-history plots are presented in Table II and Figure 5. A total of 40 measurements are used for the implementation of the Lypaunov controller: 20 total accelerations at the deck level and 20 total accelerations at the abutments at the nonlinear damper locations. The sensor locations are shown in Figure 2. The velocities are obtained by means of a second-order filter that approximates an integrator [7]. The simulations are performed within the control implementation framework set forth in the benchmark definition

DOI: 10.1002/stc

Table I. Performance indices.

Peak base shear*	Peak overturning moment*	Peak mid-span displacement*
$J_1 = \max\left\{\frac{\max_{i,t}\lvert F_b(t)\rvert}{F_{0b}^{\max}}\right\}$	$J_2 = \max\left\{\frac{\max_{i,t}\lvert M_b(t)\rvert}{M_{0b}^{\max}}\right\}$	$J_3 = \max\left\{\frac{\max_{i,t}\lvert y_m(t)\rvert}{y_{0m}^{\max}}\right\}$
Peak mid-span acceleration*	Peak bearing deformation*	Peak column curvature
$J_4 = \max\left\{\frac{\max_{i,t}\lvert \ddot{y}_m(t)\rvert}{\ddot{y}_{0m}^{\max}}\right\}$	$J_5 = \max\left\{\frac{\max_{i,t}\lvert y_b(t)\rvert}{y_{0b}^{\max}}\right\}$	$J_6 = \max\left\{\frac{\max_{j,t}\lvert \Phi(t)\rvert}{\Phi^{\max}}\right\}$
Peak dissipated energy*	♯ of plastic connections*	Normed base shear*
$J_7 = \max\left\{\frac{\max_{j,t}\int \mathrm{d}E}{E^{\max}}\right\}$	$J_8 = \max\left\{\frac{N_d^c}{N_d}\right\}$	$J_9 = \max\left\{\frac{\max_{i,t}\lVert F_b(t)\rVert}{\lVert F_{0b}^{\max}\rVert}\right\}$
Normed overturning moment*	Normed mid-span displacement*	Normed mid-span acceleration*
$J_{10} = \max\left\{\frac{\max_{i,t}\lVert M_b(t)\rVert}{\lVert M_{0b}^{\max}\rVert}\right\}$	$J_{11} = \max\left\{\frac{\max_{i,t}\lVert y_m(t)\rVert}{\lVert y_{0m}^{\max}\rVert}\right\}$	$J_{12} = \max\left\{\frac{\max_{i,t}\lVert \ddot{y}_m(t)\rVert}{\lVert \ddot{y}_{0m}^{\max}\rVert}\right\}$
Normed bearing deformation*	Normed column curvature*	Peak control force‡
$J_{13} = \max\left\{\frac{\max_{i,t}\lVert y_b(t)\rVert}{\lVert y_{0b}^{\max}\rVert}\right\}$	$J_{14} = \max\left\{\frac{\max_{j,t}\lVert \Phi(t)\rVert}{\lVert \Phi^{\max}\rVert}\right\}$	$J_{15} = \max\left\{\frac{\max_{l,t}\lvert f_l(t)\rvert}{W}\right\}$
Peak device stroke§	Peak instantaneous power	Peak total power
$J_{16} = \max\left\{\frac{\max_{l,t}\lvert d_l(t)\rvert}{x_{0m}^{\max}}\right\}$	$J_{17} = \max\left\{\frac{\max_t[\sum_l P_l(t)]}{\dot{x}_{0m}^{\max} W}\right\}$	$J_{18} = \max\left\{\frac{\sum_l \int_0^{t_f} P_l(t)\,\mathrm{d}t}{x_{0m}^{\max} W}\right\}$
♯ Control devices	♯ Sensors	Computational resources†
$J_{19} = \sharp$Devices	$J_{20} = $ Sensors	$J_{21} = \dim(x_k^c)$

*The denominator consists of the corresponding response quantity in the uncontrolled case; $i = 1,2$ for x and y directions, $j = 1, \ldots, N_d$ are the number of plastic hinges, l is the number of control devices.
†$W =$ Weight.
‡$x_{0m} = \sqrt{\Sigma y_{0b}^2}$.
§Dimension of the discrete state vector.

Table II. Performance indices for Lyapunov semiactive control.

	NPalmspr	Chi^2	El centro	Rinaldi	Turk-Bolu	Kobe-NIS
J1: Pk. base shear	0.92	0.92	0.76	0.90	0.83	0.89
J2: Pk. over. mom.	1.03	0.89	0.71	0.86	0.87	0.85
J3: Pk. mid. disp.	0.56	0.74	0.36	0.69	0.36	0.26
J4: Pk. mid. acc.	1.57	1.13	1.35	1.34	1.15	1.91
J5: Pk. bear. def.	0.56	0.74	0.35	0.70	0.38	0.27
J6: Pk. ductility	1.03	0.89	0.71	0.86	0.87	0.85
J7: Dis. energy	0.00	0.00	0.00	0.00	0.00	0.00
J8: Plas. connect.	0.00	0.00	0.00	0.00	0.00	0.00
J9: Nor. base shear	0.67	1.01	0.54	0.74	0.43	0.53
J10: Nor. over. mom.	0.66	1.00	0.51	0.70	0.42	0.52
J11: Nor. mid. disp.	0.43	0.90	0.32	0.46	0.32	0.28
J12: Nor. mid. acc.	1.59	1.58	1.23	1.24	1.13	1.19
J13: Nor. bear. def.	0.42	0.91	0.33	0.46	0.34	0.28
J14: Nor. ductility	0.66	1.00	0.51	0.70	0.42	0.52
J15: Pk. con. force	0.01	0.01	0.01	0.01	0.01	0.01
J16: Pk. stroke	0.56	0.74	0.35	0.70	0.38	0.27
J17: Pk. power	–	–	–	–	–	–
J18: Total power	–	–	–	–	–	–
J19: No. con. devices	20	20	20	20	20	20
J20: No. sensors	40	40	40	40	40	40
J21: Comp. resources	–	–	–	–	–	–

DOI: 10.1002/stc

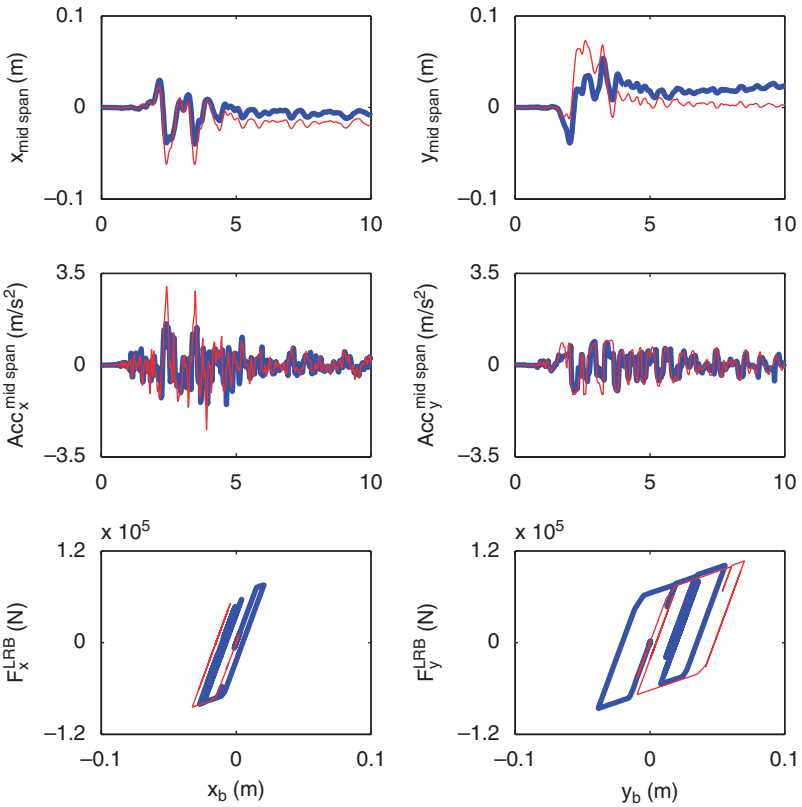

Figure 5. Comparison of Lyapunov semiactive control (thick line) and passive control (thin line) for the case of North Palm springs (1986) earthquake.

paper [31]. In addition to the semiactive control, two passive strategies are also studied for comparison purposes: (1) the MR dampers are set at their highest level of damping (essentially behaving like a passive damper and referred to hence forth as passive on case) and (2) the nonlinear damper described earlier is used instead of the MR dampers. The results of the passive case with the MR damper (MR damper passive on case) are summarized in Table III and the response quantities with the nonlinear damper are given in Table IV. The time-history results (North Palm Springs earthquake) of the mid-span displacement, mid-span acceleration and force displacement loop for the LRB are shown in Figure 5.

The advantage of semiactive Lyapunov control (Table II) is evident from the significant reductions observed in the base displacements. The reduction in mid-span displacements is about 25–74% compared with 12–76% for the MR damper passive on case and 9−50% for the nonlinear damper case. The reductions in the mid-span displacements for the MR damper passive on case occur at the cost of increased base shears and increased mid-span accelerations; however, the increases in the semiactive control case are less than those in the passive damping case. The magnitude of reductions in the mid-span displacements for the semiactive case is more than that of the nonlinear damper case. However, it can be seen that the mid-span accelerations are increased in all cases with respect to the uncontrolled case. This is because of the increased

DOI: 10.1002/stc

Table III. Performance indices for MRD–passive on.

	NPalmspr	Chi^2	El centro	Rinaldi	Turk-Bolu	Kobe-NIS
J1: Pk. base shear	1.08	1.06	0.71	1.27	1.22	0.91
J2: Pk. over. mom.	1.16	1.07	0.72	1.28	1.25	1.04
J3: Pk. Mid. disp.	0.76	0.87	0.27	0.64	0.49	0.24
J4: Pk. mid. acc.	2.98	1.46	1.77	1.39	1.42	2.69
J5: Pk. bear. def.	0.70	0.86	0.26	0.65	0.50	0.23
J6: Pk. ductility	1.16	1.07	0.72	1.28	1.25	1.04
J7: Dis. energy	0.00	0.00	0.00	0.00	0.00	0.00
J8: Plas. connect.	0.00	0.00	0.00	0.00	0.00	0.00
J9: Nor. base shear	0.76	0.86	0.77	1.11	0.39	0.60
J10: Nor. over. mom.	0.76	0.85	0.76	1.08	0.39	0.59
J11: Nor. mid. disp.	0.36	0.59	0.11	0.61	0.16	0.13
J12: Nor. mid. acc.	2.21	2.07	1.55	1.70	1.38	1.61
J13: Nor. bear. def.	0.34	0.60	0.10	0.62	0.16	0.12
J14: Nor. ductility	0.76	0.85	0.76	1.08	0.39	0.59
J15: Pk. con. force	0.01	0.01	0.01	0.01	0.01	0.01
J16: Pk. stroke	0.70	0.86	0.26	0.65	0.50	0.23
J17: Pk. power	–	–	–	–	–	–
J18: Total power	–	–	–	–	–	–
J19: No. con. devices	20	20	20	20	20	20
J20: No. sensors	40	40	40	40	40	40
J21: Comp. resources	–	–	–	–	–	–

Table IV. Performance indices for passive nonlinear damper.

	NPalmspr	Chi^2	El centro	Rinaldi	Turk-Bolu	Kobe-NIS
J1: Pk. base shear	1.06	0.91	0.62	1.07	0.78	0.91
J2: Pk. over. mom.	1.10	0.95	0.61	1.04	0.70	0.90
J3: Pk. mid. disp.	0.87	0.76	0.50	0.90	0.59	0.83
J4: Pk. mid. acc.	1.17	1.13	1.09	1.05	0.92	1.16
J5: Pk. bear. def.	0.88	0.76	0.49	0.90	0.56	0.83
J6: Pk. ductility	1.10	0.95	0.61	1.04	0.70	0.90
J7: Dis. energy	0.00	0.00	0.00	0.00	0.00	0.00
J8: Plas. connect.	0.00	0.00	0.00	0.00	0.00	0.00
J9: Nor. base shear	1.19	0.98	0.61	0.84	0.58	0.97
J10: Nor. over. mom.	1.21	0.98	0.60	0.82	0.58	0.96
J11: Nor. mid. disp.	1.02	0.98	0.59	0.76	0.52	0.96
J12: Nor. mid. acc.	0.91	1.19	0.95	0.98	0.87	0.99
J13: Nor. bear. def.	1.03	0.98	0.62	0.76	0.52	0.96
J14: Nor. ductility	1.21	0.98	0.60	0.82	0.58	0.96
J15: Pk. con. force	0.00	0.00	0.00	0.00	0.00	0.00
J16: Pk. stroke	0.88	0.76	0.49	0.90	0.56	0.83
J17: Pk. power	0	0	0	0	0	0
J18: Total power	0	0	0	0	0	0
J19: No. con. devices	20	20	20	20	20	20
J20: No. sensors	0	0	0	0	0	0
J21: Comp. resources	0	0	0	0	0	0

DOI: 10.1002/stc

Table V. Uncontrolled response quantities.

	NPalmspr	Chi^2	El centro	Rinaldi	Turk-Bolu	Kobe-NIS
$F_{0b}^{\max}$ (N)	6.934e5	1.049e6	9.950e5	1.226e6	1.108e6	7.833e5
$M_{0b}^{\max}$ (Nm)	3.268e6	6.884e6	7.330e6	8.033e6	8.001e6	5.068e6
$y_{0m}^{\max}$ (m)	0.097	0.537	0.251	0.543	0.324	0.276
$\ddot{y}_{0m}^{\max}$ (m/s^2)	1.007	1.614	1.127	2.055	1.852	0.973
$y_{0b}^{\max}$ (m)	0.103	0.544	0.249	0.550	0.328	0.286
$\Phi^{\max}$	1.563e−4	3.292e−4	3.505e−4	3.842e−4	3.826e−4	2.424e−4
$E^{\max}$	0	0	0	0	0	0
N_d	0	0	0	0	0	0
$\|F_{0b}^{\max}\|$ (N)	1.954e5	3.351e5	3.029e5	4.273e5	5.866e5	3.341e5
$\|M_{0b}^{\max}\|$ (Nm	1.365e6	2.454e6	2.211e6	3.119e6	4.286e6	2.435e6
$\|y_{0m}^{\max}\|$ (m)	0.050	0.144	0.118	0.150	0.246	0.133
$\|\ddot{y}_{0m}^{\max}\|$ (m/s^2)	0.192	0.286	0.305	0.584	0.327	0.301
$\|y_{0b}^{\max}\|$ (m)	0.054	0.147	0.120	0.149	0.252	0.141
$\|\Phi^{\max}\|$	6.526e−5	1.1734e−4	1.058e−4	1.491e−4	2.050e−4	1.1643e−4
$x^{\max}$ (m)	0.103	0.544	0.249	0.550	0.328	0.286
$\dot{x}^{\max}$ (m/s)	0.466	1.382	0.406	1.558	1.029	0.561

coupling between the deck and the relatively stiff center columns due to the addition of nonlinear dampers. Similar increases in superstructure accelerations for nonlinear base-isolated structures have also been reported in the first-generation base-isolated benchmark [28]. The uncontrolled quantities for the highway bridge are summarized in Table V for reference. It is worth noting that the sample controllers presented are not meant to be competitive and hence further reductions are possible in the semiactive control case with better control algorithms.

CONCLUSIONS

In this paper, sample passive and semiactive control strategies are presented for the Phase II highway bridge benchmark. The semiactive controller is implemented using MR dampers and a nonlinear Lyapunov control algorithm. The isolation system considered in this study consists of lead rubber bearings exhibiting bilinear hysteresis. The Lyapunov semiactive controller is developed for a system with time-varying damping. The results of the simulation study are presented in the form of a set of performance indices. It is shown that the Lyapunov semiactive controller is effective in reducing the base displacements. The control design presented in this study is intended as an aid for the benchmark problem participants; it is expected that results can be improved further by designing more effective controllers.

ACKNOWLEDGEMENTS

The authors would like to acknowledge part of the funding for this research provided by National Science Foundation CAREER grant CMS 9996290 and CMS 0099895. The second author would like to thank

DOI: 10.1002/stc

Natural Sciences and Engineering Research Council of Canada (NSERC) for their financial support through their Discovery Grants Program.

REFERENCES

1. Feng MQ, Kim JM, Shinozuka M, Purasinghe R. Viscoelastic dampers at expansion joints for seismic protection of bridges. *Journal of Bridge Engineering* 2000; **5**(1):67–74.
2. Gavin HP. Control of seismically excited vibration using electrorheological materials and lyapunov methods. *IEEE Transactions on Automatic Control* 2001; **9**(1):27–36.
3. Kawashima K, Unjoh S. Seismic response control of bridges by variable dampers. *Journal of Structural Engineering* 1994; **120**(9):2583–26901.
4. Madden GJ, Symans MD, Wongprasert N. Experimental verification of seismic response of building frame with adaptive sliding base-isolation system. *Journal of Structural Engineering* 2002; **128**(8):1037–1045.
5. Makris N, Zhang J. Structural characterization and seismic response analysis of a highway overcrossing equipped with elastomeric bearings and fluid dampers: a case study. *Report No. PEER-2002-17*, Pacific Earthquake Engineering Research Center, University of California, Berkeley, CA, 2002.
6. Nagarajaiah S, Mao YQ, Sahasrabudhe S. Nonlinear, seismic response spectra of smart sliding isolated structures with independently variable MR dampers and variable stiffness SAIVS system. *Journal of Structural Engineering and Mechanics* 2006; **24**(3):375–393.
7. Nagarajaiah S, Narasimhan S. Smart base isolated benchmark building. Part II: Phase I sample controllers for linear isolation system. *Journal of Structural Control and Health Monitoring* 2006; **13**(2–3):589–604.
8. Nagarajaiah S, Saharabudhe S. Seismic response control of smart sliding isolated buildings using variable stiffness systems: experimental and numerical study. *Earthquake Engineering and Structural Dynamics* 2005; **35**(2):177–197.
9. Nagarajaiah S, Narasimhan S. Seismic control of smart base isolated buildings with new semiactive variable damper. *Earthquake Engineering and Structural Dynamics* 2007; **36**(6):729–749.
10. Narasimhan S, Nagarajaiah S. STFT algorithm for semiactive control of base isolated buildings with variable stiffness isolation systems subjected to near fault earthquakes. *Engineering Structures* 2005; **27**:514–523.
11. Narasimhan S, Nagarajaiah S. Smart base isolated buildings with variable friction systems: H_∞ controller and novel SAIVF device. *Earthquake Engineering and Structural Dynamics* 2006; **35**(8):920–942.
12. Narasimhan S, Nagarajaiah S, Johnson EA, Gavin HP. Smart base isolated benchmark building. Part I: problem definition. *Journal of Structural Control and Health Monitoring* 2006; **13**(2–3):573–588.
13. Saharabudhe S, Nagarajaiah S. Effectiveness of variable stiffness systems in base isolated bridges subjected to near fault earthquakes: experimental study. *International Journal of Intelligent Material Systems and Structures* 2005; **16**(9):743–756.
14. Sahasrabudhe S, Nagarajaiah S. Semi-active control of sliding isolated bridges using MR dampers: an experimental and numerical study. *Earthquake Engineering and Structural Dynamics* 2005; **34**(8):965–983.
15. Spencer BF, Johnson EA, Ramallo JC. Smart isolation for seismic control. *JSME International Journal Series C* 2000; **43**(3):704–711.
16. Spencer BF, Nagarajaiah S. State of the art of structural control. *Journal of Structural Engineering* 2003; **129**(7):845–856.
17. Tsopelas P, Constantinou MC. Study on elastoplastic bridge seismic isolation system. *Journal of Structural Engineering* (ASCE) 1997; **123**(4):489–498.
18. Turkington DH, Carr AJ, Cooke N, Moss PJ. Seismic design of bridges on lead-rubber bearings. *Journal of Structural Engineering* (ASCE) 1988; **115**:3000–3016.
19. Yang JN, Wu JC, Kawashima K, Unjoh S. Hybrid control of seismic excited bridge structures. *Earthquake Engineering and Structural Dynamics* 1995; **24**:1437–1451.
20. Yang JN, Wu JC, Reinhorn A, Riley M. Control of sliding-isolated buildings using sliding-mode control. *Journal of Structural Engineering* (ASCE) 1995; **122**:179–186.
21. Spencer Jr BF, Dyke SJ, Deoskar HS. Benchmark problems in structural control—Part I: active mass driver system. *Earthquake Engineering and Structural Dynamics* 1998; **27**(11):1127–1139.
22. Spencer Jr BF, Dyke SJ, Deoskar HS. Benchmark problems in structural control—Part II: active tendon system. *Earthquake Engineering and Structural Dynamics* 1998; **27**(11):1141–1147.
23. Yang JN, Agrawal AK, Samali B, Wu JC. A benchmark problem for response control of wind excited tall buildings. *Journal of Engineering Mechanics* 2004; **130**(4):437–446.
24. Ohtori Y, Christenson RE, Spencer BF, Dyke SJ. Benchmark control problems for seismically excited nonlinear buildings. *Journal of Engineering Mechanics* (ASCE) 2004; **130**(4):366–385.
25. Dyke SJ, Caicedo JM, Turan G, Bergman LA, Hague S. Phase 1: benchmark control problem for seismic response of cable-stayed bridges. *Journal of Structural Engineering* (ASCE) 2003; **129**(7):857–872.

DOI: 10.1002/stc

26. Caicedo JM, Dyke SJ, Moon SJ, Bergman LA, Turan G, Hague S. Phase II benchmark control problem for seismic response of cable-stayed bridges. *Journal of Structural Control* 2003; **10**(3–4):137–168.
27. Erkus B, Johnson E. Smart base isolated benchmark building. Part III: a sample controller for bilinear isolation. *Journal of Structural Control and Health Monitoring* 2006; **13**(2–3):605–625.
28. Narasimhan S, Nagarajaiah S, Johnson EA. Smart base isolated benchmark building. Part IV: Phase II sample controller for nonlinear isolation systems. *Journal of Structural Control and Health Monitoring* 2008; **15**(5):657–672.
29. Narasimhan S, Nagarajaiah S, Johnson E. Structural control benchmark problem: Phase II—nonlinear smart base-isolated building subjected to near-fault earthquakes. *Structural Health Monitoring and Control* 2008; **15**(5):653–656.
30. Yang JN, Agrawal AK. Semi-active hybrid control systems for nonlinear buildings against near-field earthquakes. *Engineering Structures* 2002; **24**(3):271–280.
31. Agrawal AK, Tan P, Nagarajaiah S, Zhang J. Benchmark structural control problem for a highway bridge. *Journal of Structural Control and Health Monitoring* 2008; DOI: 10.1002/stc.300.
32. Tan P, Agrawal AK. Benchmark structural control problem for a seismically excited highway bridge, Part II: Phase I sample control designs. *Journal of Structural Control and Health Monitoring* 2008; DOI: 10.1002/stc.301.
33. Carlson JD, Chrzan MJ. 1994. Magnetorheological fluid dampers. *U.S. Patent No. 5,277,281*.
34. Spencer BF, Dyke SJ, Sain MK, Carlson JD. Phenomenological model of a magnetorheological damper. *Journal of Engineering Mechanics* 1997; **123**(3):230–238.
35. ABAQUS. *Hibbit*. Karlsson & Sorensen Inc.: Pawucket, RI, 2003.
36. Park YJ, Wen YK, Ang AHS. Random vibration of hysteretic systems under bi-directional ground motions. *Earthquake Engineering and Structural Dynamics* 1986; **14**(4):543–557.